

UC Irvine

ICTS Publications

Title

Wide-field functional imaging of blood flow and hemoglobin oxygen saturation in the rodent dorsal window chamber.

Permalink

<https://escholarship.org/uc/item/6228w10r>

Journal

Microvascular research, 82(3)

ISSN

1095-9319

Authors

Moy, Austin J
White, Sean M
Indrawan, Elmer S
[et al.](#)

Publication Date

2011-11-23

Peer reviewed



Published in final edited form as:

Microvasc Res. 2011 November ; 82(3): 199–209. doi:10.1016/j.mvr.2011.07.004.

Wide-field Functional Imaging of Blood Flow and Hemoglobin Oxygen Saturation in the Rodent Dorsal Window Chamber

Austin J. Moy^{a,b}, Sean M. White^{a,b}, Elmer S. Indrawan^{a,b}, Justin Lotfi^a, Matthew J. Nudelman^a, Samantha J. Costantini^a, Nikita Agarwal^c, Wangcun Jia^a, Kristen M. Kelly^a, Brian S. Sorg^c, and Bernard Choi^{a,b,*}

^aBeckman Laser Institute, University of California, Irvine, 1002 Health Sciences Road East, Irvine, CA 92612

^bDepartment of Biomedical Engineering, University of California, Irvine, 3120 Natural Sciences II, Irvine, CA 92697

^cDepartment of Biomedical Engineering, University of Florida, P.O. Box 116131, Gainesville, FL 32611

Abstract

The rodent dorsal window chamber is a widely used *in vivo* model of the microvasculature. The model consists of a 1cm region of exposed microvasculature in the rodent dorsal skin that is immobilized by surgically implanted titanium frames, allowing the skin microvasculature to be visualized. We describe a detailed protocol for surgical implantation of the dorsal window chamber which enables researchers to perform the window chamber implantation surgery. We further describe subsequent wide-field functional imaging of the chamber to obtain hemodynamic information in the form of blood oxygenation and blood flow on a cm size region of interest. Optical imaging techniques, such as intravital microscopy, have been applied extensively to the dorsal window chamber to study microvascular-related disease and conditions. Due to the limited field of view of intravital microscopy, detailed hemodynamic information typically is acquired from small regions of interest, typically on the order of hundreds of μm . The wide-field imaging techniques described herein complement intravital microscopy, allowing researchers to obtain hemodynamic information at both microscopic and macroscopic spatial scales. Compared with intravital microscopy, wide-field functional imaging requires simple instrumentation, is inexpensive, and can give detailed metabolic information over a wide field of view.

Keywords

Microvasculature; window chamber; surgery; optical imaging; laser speckle; multispectral imaging

© 2011 Elsevier Inc. All rights reserved.

*Corresponding author: Bernard Choi, Beckman Laser Institute, University of California, Irvine, 1002 Health Sciences Road East, Irvine, CA 92612. Fax: 1-949-824-6969. choib@uci.edu.

Publisher's Disclaimer: This is a PDF file of an unedited manuscript that has been accepted for publication. As a service to our customers we are providing this early version of the manuscript. The manuscript will undergo copyediting, typesetting, and review of the resulting proof before it is published in its final citable form. Please note that during the production process errors may be discovered which could affect the content, and all legal disclaimers that apply to the journal pertain.

INTRODUCTION

The rodent dorsal window chamber is an *in vivo* model that has been an invaluable technique in studying the microvasculature over the last thirty years. The concept of the dorsal window chamber was first described in 1943 (Algire, 1943). Other early iterations of the dorsal window chamber have been described in rats (Papenfuss et al., 1979), and consisted of a segment of dorsal skin secured between two aluminum frames. One full skin thickness of the skinfold was then removed, exposing the microvasculature on the fascial side of the opposing full thickness of skin.

Modifications have since been made to the originally published protocol to increase efficiency of the procedure as well as adapt the model for use on smaller rodents, such as mice and hamsters (Endrich et al., 1980; Lehr et al., 1993). The original aluminum chambers have been replaced by titanium or, in some instances, lightweight polymers (Gaustad et al., 2008). Titanium frames reduce heat loss, ensure biological inertness, and have enhanced physical stability compared to their aluminum chamber predecessors (Lehr et al., 1993).

The dorsal window chamber has found utility in many biomedical research applications, notably in studies of angiogenesis (Dellian et al., 1996; Laschke and Menger, 2007) and tumor progression, evaluation of microvascular-targeted biomolecular therapies (Yuan et al., 1996), evaluation of cryosurgical destruction on human prostate cancer (Chao et al., 2004; Jiang et al., 2008), evaluation of light-based therapies targeting the microvasculature (Choi et al., 2008), and evaluation of topically applied chemical enhancement of light-based therapy (Vargas et al., 2008). Tumor studies have been performed via implantation of tumor cell lines or primary tumor cells into the dorsal window chamber, allowing for direct visualization of the entire tumor and the surrounding vasculature (Dewhirst et al., 2000; Jain et al., 2002). The window chamber model also has been modified to allow for the study of other tissues. Studies have been performed utilizing the dorsal window chamber to isolate muscle tissue within the window chamber and evaluate the interaction of leukocyte and endothelial cells after muscle damage (Øye et al., 2008).

The primary advantage of the dorsal window chamber is that its use enables longitudinal *in vivo* imaging of the microvasculature in order to answer questions about its role in normal and diseased conditions. Intravital fluorescence microscopy often is used to visualize the microvasculature within the window chamber (Khurana et al., 2008; Lehr et al., 1993). This technique typically utilizes a reporter molecule expressed by cells of the microvasculature, like endothelial cells (Chishima et al., 1997; Fukumura et al., 1998), or a fluorescent dye typically used to label the plasma (Wu et al., 1997), such as a fluorescent protein or a dye, with a particular excitation and emission spectrum. Other studies using intravital microscopic imaging of the dorsal window chamber include tumor hypoxia (Dewhirst et al., 1999), tumor vascular permeability (Dreher et al., 2006), tumor necrosis factor (Seynhaeve et al., 2007), and angiogenesis (Peirce et al., 2004).

The aforementioned examples from the literature demonstrated the utility of the dorsal window chamber in many biomedical applications, and in particular oxygenation studies, as well as the ease with which the model can be imaged. The use of intravital microscopy is best suited for imaging small regions of interest, typically in the hundreds of μm . The ability to obtain hemodynamic information from larger regions of interest with intravital microscopy, however, is largely impractical. We introduce in this paper a complementary technique and protocol to perform wide-field functional imaging of the dorsal window chamber, to study hemoglobin oxygenation and blood flow from within the exposed vasculature. Previous studies (Choi et al., 2008; Choi et al., 2004; Dedeugd et al., 2009; Sorg et al., 2008; Sorg et al., 2005) showed that wide-field functional imaging of the dorsal

window chamber can provide repeatable, quantitative information about hemodynamics in a non-invasive manner and has great utility in other laboratory studies. Before discussing wide-field functional imaging, we first describe in detail a window chamber surgical protocol which has worked well in our laboratories at the University of California, Irvine and University of Florida.

MATERIALS

Parts	Tools
2x Titanium dorsal window chamber (Fig. 1A)	Small Phillips screwdriver
2x Titanium dorsal window chamber (Fig. 1A)	Electric hair clippers
3x Phillips stainless steel machine screw (0-80 gauge, 5/16" length) (Fig. 1A)	1x C-clamp with 2 large screws + nuts (optional) (Fig. 1B and Fig. 1C)
3x Spacer (0-80 gauge, 2 mm length, 3/32" outer diameter) (Fig. 1A)	Hole puncher (optional)
3x Stainless steel machine screw hex nut (0-80 Thread Size, 5/32" Width, 3/64" Height) (Fig. 1A)	
1x Glass cover slip, size #2	
1x Plastic cover slip retaining ring	

Supplies/Reagents	Surgical Instruments
4-0 suture	Forceps
Depilatory cream or lotion	Hemostats
Sterile saline	Surgical curved iris scissors
Sterile alcohol prep pads	Sterilizer (autoclave or dry-bead)
Sterile cotton swabs	
Sterile artificial tears	
Surgical towels	
Anesthetic cocktail (Ketamine/Xylazine)	

Pre-Surgical Preparation

Surgeon Preparation—Hands should be scrubbed and dried with sterile towels. Surgeon should wear sterile scrubs, shoe covers, hair net, mask, surgical gown, and sterile gloves.

Assembly of window chamber frame—One side of the window chamber frame should be pre-assembled with spacers and screws prior to installation. The window chamber can be assembled before sterilization so it is ready to be installed at the time of surgery.

Sterilization of components, instruments, and tools—Sterilize chamber components and surgical and window chamber tools using a dry-bead sterilizer. (alternatively, an autoclave can also be used for sterilization)

Notes: For tools with temperature-sensitive parts (e.g., screwdriver with a plastic handle), ethylene-oxide gas sterilization or dry bead sterilization of metal parts that come in contact with the window chamber or animal can be used. If a dry bead sterilizer is used, disinfect the handle of the tool with 70% ethanol or a commercial disinfectant such as Sporicidin®.

Preparation of surgical area—The laboratory surgical area should be in a generally isolated location. Disinfect the surgery area using a solution of 4% bleach or a commercial product such as Sporidicin®. Countertops, surgical platforms, and any support surfaces should be wiped down. Place a tray of sterilized tools within reach in the surgical area, and cover a pre-warmed heating pad in the surgery area with a sterile drape. Optionally, a solution of warm (35-37°C) sterile saline can be placed near the surgery area to rinse the tool. A sterile, covered glass Petri dish placed on a hot plate serves this purpose.

PROCEDURE

Animal preparation

1) Place the animal in a gas anesthesia chamber filled with 5% isoflurane in 100% O₂ until the animal stops moving. Leave the animal in the chamber for an additional 1-2 minutes, then remove the animal from the chamber and position its snout in a nose cone that is continuously delivering 1-2% isoflurane in 100% O₂.

Notes: Alternatively, an anesthetic cocktail, such as ketamine/xylazine, can be administered via intraperitoneal (i.p) injection. While this method allows for easier manipulation of the animal during surgery, recovery time is much longer than with gas anesthesia. Conversely, using gas anesthesia can impede the surgeon's ability to manipulate the animal.

2) Once the animal is anesthetized, lubricate its eyes with a sterile ophthalmic ointment to prevent corneal dehydration. This should be repeated as necessary during the procedure.

3) If the animal has hair, use small animal electric clippers to remove coarse dorsal hair along the length of the animal from the hind legs up to the ears followed by application of a commercial depilatory cream or lotion (i.e. Nair) to remove fine hair.

Notes: Maintaining a sterile environment minimizes the risk of infection and promotes window chamber longevity. This is especially important if immune system-compromised animals are used. If desired, the bare skin of the surgical site can also be cleaned and sanitized with a surgical scrub containing povidone iodine followed by 70% ethanol. For sterile handling of the animal, a small sterile fenestrated drape can be wrapped around the animal with the opening placed over the surgical site.

Dorsal skin traction

4) The dorsal skin must be secured to facilitate attachment of the window chamber apparatus. Hamster: Gently but securely pinch the dorsal skin in the C-clamp. (Fig. 2)

Mice: Gently stretch the dorsal skin with the fingers and hold in place during chamber installation as outlined below.

5) Mice have less skin to work with than hamsters, so it is critically important to use mice of sufficient size. Mice of minimum 21g body mass can be used, though mice of 25g or greater are recommended.

6) Once the animal skin is securely held in place, transilluminate the skin with a standard white light source to enable visualization of the surgical field and the location of blood vessels and other dermal structures.

7) Place one half of the window chamber flat on the animal skin at the desired incision location. Maneuver the window chamber for optimal placement. Use a skin marker to mark

the eventual location of the holes used for screw placement. The titanium window chamber can be used as a template (Fig. 3).

Surgical installation of window chamber frame

8) Create the window chamber screw holes.

Hamster: First use a leather belt hole puncher on the smallest setting (<2mm diameter) to make the initial incision. Then use sharp tipped scissors to widen the hole by inserting the closed blades into the hole and carefully expanding the blades of the scissors.

Mice: Use a large gauge needle (18 or 16 gauge) to make the initial incision and use scissors to expand the incision if necessary.

Critical notes: The holes need to be sufficiently large to accommodate the window chamber spacers, but not so large that saline can leak out of the window chamber through the holes.

9) Place the screws of the pre-assembled half of the window chamber through the screw holes in the skin. The screws should poke through the skin thickness that will remain intact, and the spacers should lie directly in the screw holes to minimize the potential for infection. With forceps, remove any remaining connective tissue attached to the screws.

10) Place the second half of the window chamber support frame on the set screws and position flush with the spacers.

11) Secure the window chamber frames with a nut placed on each screw.

12) Once secured, suture the frames in place with 4-0 suture. There are four suture holes on each side of the central support screw at the top of the frame (total of eight suture holes on top) and three suture holes next to each of the two screws at the bottom of the frame (total of six holes on bottom). Loop suture through two adjacent suture holes at the top of the window frame for a total of four suture loops at the top, and through the outer two adjacent holes at the bottom of the frame for a total of two sutures loops at the bottom.

Hamster only: The C-clamp used for fixation of the dorsal skin for attachment of the window chamber support frames can be removed prior to suture placement. Removing the C-clamp allows for easier manipulation during suturing, but care should be taken to prevent the skin from shifting during suturing.

Window chamber incision

13) With fine-pointed forceps, gently pinch a small section at the boundary of the skin to be removed and make a small incision with the surgical scissors on the incision boundary.

14) Use the forceps to lift the skin around the cut so that one blade of the scissors can be inserted to make the incision. Carefully begin making a circular incision; this is the piece of skin that will be removed to create the window. It is important to make the cut with a slightly smaller diameter than the actual window size as the skin will stretch to create a larger opening. The skin can be trimmed to make a larger opening if needed (Fig. 4).

15) Once the skin is removed, the exposed microvasculature must be kept moist. Use a 1mL tuberculin syringe without needle or 1mL plastic Pasteur pipette to place a few drops of warm sterile saline onto the exposed site. The site should be periodically moistened with saline throughout the surgical procedure.

16) After the skin is removed, remove the remaining fascia from the exposed site. Use fine sharp-tipped forceps to carefully and gently lift the fascia off. Once the fascia is stretched tight, remove the fascia with a curved pair of sharp-tipped scissors. Repeat this process until the site is cleared of remaining fascia.

Notes: Fascia removal is critical to improve imaging and promote longevity of the window chamber, but must be done carefully to avoid damage to the underlying tissue. Any remaining fascia will generally appear as small raised clumps of tissue in the exposed site. It is very important to avoid pinching or touching the site as this may damage the tissue and microvasculature, which can result in hemorrhage and decreased optical clarity of the window.

Alternate procedure to perform skin incision and window chamber frame installation—An alternate procedure can be performed in which the window chamber frames are attached after making the skin incision. If this protocol is desired, simply perform steps 13-16 prior to steps 8-12.

There are pros and cons for both procedures. It is easier to make the skin incision and clean the wound site without the window chamber frame in place, but there is higher risk for creating an incorrectly sized incision or for an inconvenient shift in the incision position after suturing the window chambers in place. If the incision is made after placement of the window chamber, then the exact size and placement of the incision will be obtained, but it is more difficult to remove all overlying skin from the window chamber. We believe that it takes more experience to correctly make the incision prior to attachment of the window chamber.

[OPTIONAL] Implantation of tumor cells: If a tumor will not be initiated in the window chamber, then this step can be skipped.

17) Initiation of a tumor in the window chamber can be accomplished with superficial injection of a suspension of tumor cells in the dermis of the window chamber skin. A tumor cell suspension in serum-free growth medium should be prepared prior to window chamber surgery and placed on ice during surgery. An injection volume of 10 μ L is recommended. The concentration of cells in the tumor cell solution should be adjusted to deliver the desired number of total cells in the injection volume. Depending on the origin of the tumor cells (rodent, human) and the animal model (immunocompromised, etc.) we have found that anywhere from 5 \times 10³-5 \times 10⁵ cells are sufficient to establish a tumor that will reach 2-3mm diameter after 7-10 days post implantation.

Injection of the 10 μ L volume of tumor cells can be accomplished using a precision syringe. We have had success with 1mL Hamilton gas-tight glass syringes (Hamilton Company, Reno, NV) with a luer tip that is fitted with a 30G 1/2-inch needle. Prior to injection, the needle is bent to a slight angle (~30°) in the direction of the bezel at the needle tip to aid in positioning of the needle in the window chamber. The needle should be inserted as superficially as possible in the exposed dermis of the incision site for optimal imaging of the developing tumor. When the injection is performed in this manner, it is possible with fluorescence imaging to image individual tumor cells which express fluorescent proteins at sufficiently low cell concentrations.

Window chamber closure and animal recovery

18) Lay the window chamber flat and overfill the chamber with saline.

19) Submerge the coverslip in the saline at an angle by inserting one edge first, then slowly lowering the coverslip into place while pushing excess fluid out of the chamber (Fig. 5).

Notes: The window chamber must be filled with saline to keep the tissue moist and the cover slip placed in such a way to avoid trapping air bubbles. Our window chambers accommodate 12mm-diameter circular cover slips. We recommend #2 size cover slips, although #1 size cover slips could be used, as they are designed for use with many microscopy systems, but are less durable.

20) Wipe away excess fluid on the outside of the coverslip, taking care not to wick away fluid underneath the coverslip.

21) Insert a retaining ring on top of the cover slip to hold it in place.

Notes: Metal or plastic rings can be used. Metal retaining rings are commercially available, while the plastic rings we use are custom made. The metal rings are very sturdy and occupy minimal space in the window chamber, but can be more difficult to handle and maneuver into place. We find the plastic rings easier to handle and position properly, but take up more space in the window chamber and reduce the viewable area of the window chamber. Additionally, some plastics are auto-fluorescent and can cause significant imaging artifacts.

22) Immediately post-surgery, inspect the window chamber to ensure that it is clean.

23) Before the animal regains consciousness, perform a subdermal injection of buprenorphine at a volume equal to 0.16% of the animal's mass into the dorsum. Buprenorphine is an analgesic that aids the animal in recovery. Afterwards, apply a topical antibiotic ointment to all suture, screw, and wound areas to help prevent infection. Animals should be placed in a quiet area on a heating pad to recover from surgery. Once the animal is ambulatory, it can be returned to housing.

In experienced hands, the entire surgical procedure for one anesthetized animal is approximately 30-40 minutes.

Window Chamber Animal Housing

Due to the presence of the window chambers on the dorsum of the animals, extra cage space is required to house these animals comfortably. As a result, one animal is housed per cage. This is especially true for mice since multiple mice with window chambers housed together will damage each other's window chambers. Extra bedding added to the cage insures that the animals can reach food hoppers and water dispensers on the cage lid.

We successfully and routinely maintain tumorless window chamber animals under standard temperature and humidity conditions with no complications. This said, specialized housing conditions can be utilized to help sustain and maintain the window chamber viability. The seal between the exposed skin and the window chamber is not complete, so moisture can escape with the potential to dry out the window chamber and render it non-viable. An increased humidity of about 50% in the housing environment can help to reduce the potential for the window chamber to dry out excessively.

Temperature is known to affect cell growth, gene expression, and physiology. For tumor-bearing window chambers, it is important that the window chamber be maintained at an appropriate housing temperature. The surgically implanted window chamber keeps the skin suspended away from the body such that the suspended skin will not be maintained at normal body temperature. Since it is no longer in direct contact with the animal body, heat will be lost to the ambient environment on both sides of the raised skin flap. To achieve a

physiologically relevant environment for tumor growth and development, it is necessary to maintain the initiated tumor and hence the skin flap as close as possible to the normal skin temperature of 33-34°C (Dewhirst et al., 2000; Endrich et al., 1979). This is possible by housing animals in a 33-34°C environment post-surgery. Previous studies have shown that the skin temperature of mouse window chambers at room temperature (25°C) was found to be lower (28.7°C) than that of animals housed at 35°C (skin temperature of 33.9°C) (Endrich et al., 1979). Tumors in the windows of mice housed at the higher temperatures were shown to grow at double the rate of those in mice housed at room temperature. In addition, the arteriolar blood supply to the tumors was increased in the tumors at the 35°C housing conditions.

Thus, as the skin temperature is affected by the ambient housing temperatures and has physiological consequences on tumor development, it is important to house animals with tumor-bearing window chambers at elevated temperatures so that the models are more physiologically relevant. These housing conditions are generally considered non-standard; therefore, exceptions to standard housing conditions must be approved by institutional animal care and use committees for protocols involving tumor-bearing window chamber animals.

Post-Surgery Window Chamber Maintenance

In order to maintain a patent and viable window chamber for as long as four weeks, it is necessary to perform periodic maintenance on the window chamber, usually once daily or every other day. Sutures frequently come undone or are chewed off by the animals and must be replaced. Antibiotic ointment should be applied whenever sutures are replaced. The nuts on the window chamber set screws can loosen and these must be retightened or replaced if lost. Bedding and other cage debris can become lodged and trapped in various places in the window chamber and must be removed. If imaging is performed frequently, then window chamber maintenance can become part of the imaging routine, otherwise, sessions for window chamber maintenance will need to be scheduled in between imaging times.

In general, these procedures can be performed relatively quickly with gas anesthesia. Gas anesthesia is strongly preferred for window chamber maintenance since it is fast acting with rapid recovery. Frequent use of injectable anesthetics, such as ketamine, can result in development of a tolerance to the drugs that complicates proper and safe dosing (Fish, 1997). In addition, frequent repeated injections of anesthesia, especially when delivered intraperitoneally to small animals like mice, can result in tissue trauma.

Wide-field Functional Imaging

Laser Speckle Imaging—Laser speckle imaging (Briers and Fercher, 1982; Fercher and Briers, 1981) is an imaging technique in biomedical optics that allows wide-field image acquisition and requires simple instrumentation. The technique utilizes the speckle pattern that is visually observed when a laser illuminates a surface to detect movement of scattering particles, like red blood cells, that are moving through the laser illumination field. As the cells move, the speckle pattern changes quickly over time with a relatively long camera exposure time. By acquiring images of the blurred speckle pattern with a camera at specified exposure times, relative blood flow information can be acquired. A recent review on the use of laser speckle imaging in biomedical optics discusses in more detail other applications of this imaging modality (Boas and Dunn, 2010).

Multispectral Imaging—Multispectral imaging involves the acquisition of images at multiple wavelengths. To calculate hemoglobin oxygenation saturation (Dunn et al., 2003; Sorg et al., 2005), absorption contrast images at multiple wavelengths are acquired and the

images differ based on the optical properties of the blood. The instrumentation in multispectral imaging is also simple, consisting of a broadband light source, camera, and filter sets for the desired wavelengths.

Animal Imaging Procedure—Animals are initially anesthetized using 5% isoflurane in 100% oxygen and kept unconscious using 1% isoflurane in 100% oxygen via a nose cone anesthesia setup [EZ-1000, E-Z Anesthesia, Palmer, PA]. The window is then immobilized against a square piece of acrylic with holes used to hold the window chamber screws. This creates a mechanically stable imaging setup that is consistent day to day and facilitates use of longitudinal imaging studies.

Laser Speckle Image Acquisition

1. Prepare the window chamber, laser illumination system, and imaging system for LSI data acquisition in either a reflection or transmission geometry. Transillumination geometry is preferred due to the fact that red blood cells are strongly forward scattering. This geometry is shown graphically in Figure 6.
 - a. The window chamber should be completely and uniformly illuminated using a diffused laser beam. A collimating lens may be necessary to achieve adequate laser intensity at the sample. A diffuser is likely necessary to homogenize the Gaussian intensity profile of the laser beam.
 - b. Speckle contrast of acquired images is optimized when the minimum size of the speckles being imaged is twice the camera pixel size (Kirkpatrick et al., 2008; Yuan et al., 2005). This additionally satisfies the Nyquist criterion. Minimum speckle size is calculated as $d = 2.44(1+M)\lambda(f/\#)$, where d is the speckle size, M is the imaging system magnification, λ is the laser wavelength, and $f/\#$ is the f-number of the imaging system.
2. For a given image exposure time, the maximum detector dynamic range should be used while avoiding detector saturation.
 - a. Pixel intensity is typically modified by adjusting the intensity of the laser illumination system via laser current adjustment, usage of neutral density filters, or usage of a polarizer-analyzer pair.
3. Acquire raw speckle images.
 - a. If spatial correlation analysis (Briers and Webster, 1996) is to be used for computation of speckle contrast, a sufficient number of images should be taken to allow noise reduction via averaging of all computed blood flow maps. Ten images are typically adequate.
 - b. If temporal correlation analysis (Cheng et al., 2003; Cheng et al., 2008) is to be used for computation of speckle contrast, a minimum of roughly 25 images should be acquired in series to achieve adequate statistical accuracy when computing speckle contrast.
4. Compute speckle contrast image from each raw speckle image.
 - a. Speckle contrast is given by:

$$K = \frac{\sigma}{\langle I \rangle}$$

Equation 1: Speckle contrast equation

where K is speckle contrast, σ is the standard deviation of a group of pixel values, and $\langle I \rangle$ is the average value of the same group of pixels.

- b. For spatial contrast analysis, a 5×5 or 7×7 sliding window is typically used to compute speckle contrast. Larger windows allow for more accurate statistical sampling at the expense of spatial resolution. This computation is performed for each acquired raw speckle image. For temporal contrast analysis, speckle contrast of a selected pixel is calculated using the values of the selected pixel from all the collected raw speckle images. This analysis is then performed over all pixels to create a single speckle contrast map. An averaging filter can then be used for speckle contrast map smoothing.

5. Compute speckle flow index image from speckle contrast images

For most practical cases, it is appropriate to calculate a speckle correlation time using the following simplified speckle imaging equation (Cheng and Duong, 2007; Ramirez-San-Juan et al., 2008):

$$\tau_c = 2TK^2 \quad \text{Equation 2: Simplified expression for correlation time}$$

This equation is valid for $K < 0.5$, which is the typical range of values for speckle contrast acquired using our LSI system. Taking the reciprocal of the correlation time gives a parameter, the speckle flow index (SFI), which is a measure of the relative blood flow:

$$SFI = \frac{1}{2TK^2} [s^{-1}] \quad \text{Equation 3: Expression for speckle flow index (SFI)}$$

SFI can be used to perform relative comparisons of blood flow between images taken at different time points and give a sense of the overall blood flow dynamics. Selection of exposure time is an important consideration and will alter the sensitivity to different perfusion velocities. An exposure time of 10 ms allows imaging of blood flow speed with a linear response in the [0-5 mm/s] range (Choi et al., 2006). Figure 7 shows pictorially the progression from the raw speckle image to the speckle contrast image, and finally to the speckle flow index map.

A detailed protocol of the imaging procedure used for hemoglobin saturation imaging is presented below. A technical discussion of the imaging system, image acquisition methods, and image processing methods was given in a previous publication (Sorg et al., 2005).

Hemoglobin Saturation Imaging

Imaging System Calibration—1. Choose the wavelengths that will be used for image acquisition. The choice will be based on the wavelength-dependent absorbance of hemoglobin and the blood vessel diameters of interest as sufficient light must be transmitted through the blood vessel in order to be imaged. In our case, we used a wavelength range of 500-575nm at 5nm intervals (16 total images acquired per dataset) to image microvessels with approximate diameters of 20-100 μ m.

2. Measure *in vitro* the extinction coefficients of cell-free oxy- and deoxyhemoglobin at the chosen wavelengths using the imaging system. This is necessary to account for various effects on the hemoglobin absorption spectrum due to the emission spectra of the illumination source, the transmission of the microscope optical elements, the detection sensitivity of the camera, and the bandwidth of spectral filtering elements, like a liquid

crystal tunable filter (LCTF), that may cause deviations from published values in the literature.

Image Acquisition—3. Acquire images in experimental animals at each of the chosen wavelengths such that the full dynamic range of the camera is used. A minimum acquisition time for each wavelength no shorter than 300ms should be used for microvessels with diameters between 20-100 μ m in order to average out random red blood cell motion that can cause fluctuations in the transmitted light which can lead to noise in the hemoglobin saturation data (Pittman and Duling, 1975; Sorg et al., 2005).

4. Image acquisition times at each wavelength can be predetermined by a trial experiment on a representative animal to find reasonable minimum image acquisition times to use. For our wavelength range the LCTF had the highest transmission at 575nm, thus the light level of the illumination source was set at this wavelength. An image acquisition time of 400ms at 575nm was used with the light levels adjusted so that the full dynamic range of the camera was employed. The image acquisition time at other wavelengths was adjusted accordingly up to a 1400ms acquisition time at 500nm. With automated LCTF tuning and image capture, acquisition of a complete data set required about 13s.

Image Processing—5. Images are processed on a pixel-wise basis using the hemoglobin calibration data and a model equation to describe light attenuation in the blood vessel. In our case, a linear least-squares regression of the data was used in the following linear mixing model (Shonat et al., 1997; Sorg et al., 2005):

$$A_{\lambda} = \log\left(\frac{I_0}{I}\right) = \epsilon_{\lambda}^{\text{HbO}_2} \cdot [\text{HbO}_2] \cdot L + \epsilon_{\lambda}^{\text{Hb-R}} \cdot [\text{Hb-R}] \cdot L + \text{SL}$$

where A_{λ} is the absorbance at wavelength λ , I is the raw pixel value, I_0 is the reference light pixel value selected from avascular regions of tissue, $\epsilon_{\lambda}^{\text{HbO}_2}$ and $\epsilon_{\lambda}^{\text{Hb-R}}$ are the extinction coefficients for oxy- and deoxyhemoglobin respectively at wavelength λ from the calibration spectra, $[\text{HbO}_2]$ and $[\text{Hb-R}]$ are the concentrations of oxy- and deoxyhemoglobin, respectively, and SL is a pathlength-dependent scattering term where scattering is assumed to be constant over the wavelength range. The scattering term functions mathematically like a constant additive error term in the linear regression.

6. The raw pixel values (I) at each wavelength are converted to absorbance values by manually selecting 3 or 4 avascular reference regions in the images to use as an estimate of I_0 . The same regions are used in each image at each wavelength, and the value used for I_0 at each wavelength is an average of the pixel values in the reference regions. Care should be taken to not select regions with any saturated pixels as this would introduce artifacts in the resulting hemoglobin saturation calculations.

7. Calculated values of hemoglobin saturation at each pixel are accepted or rejected based on the R^2 value (standard definition for the coefficient of determination) for the fit of the calculated unknowns from the data to the model. In our case, $R^2 = 0.90$ is used.

8. The pixel hemoglobin saturation data can be used to create pseudocolor images for analysis of spatio-temporal variations in microvessel hemoglobin saturation. Additionally, the pixel data can be extracted for graphical analysis of microvessel regions of interest.

Figure 8 shows how hemoglobin saturation maps are generated, starting with the creation of a reference spectra that is used calculate experimental hemoglobin saturation values in the

dorsal window chamber. Figure 9 shows an application of spectral imaging in creating hemoglobin saturation maps for a tumor initiated in a dorsal window chamber.

Instrument Configurations

LSI and multispectral imaging are performed either with individual instruments or as a single combined, multimodal instrument. Examples of both configurations are described below.

Individual Laser Speckle Imaging and Multispectral Imaging Instrumentation

—As a standalone instrument, LSI involves use of a CCD camera equipped with macro lens, coherent light source (e.g., 633-nm HeNe laser), and 150 W quartz halogen lamp for brightfield imaging. Images are acquired in either epi-illumination or transillumination geometry.

One example of a stand-alone multispectral imaging instrument is based on a standard upright microscope. The spatial resolution for the spectral imaging system is determined by a number of factors with the main factor being the objective lens used for imaging. Submicron pixel resolution is possible with this system. The temporal resolution of the spectral imaging system (~13-20s) is sufficient to measure naturally occurring fluctuations in microvessel oxygenation consistent with oxygen microelectrode recordings as reported previously (Hardee et al., 2009; Sorg et al., 2008). For our application – the imaging of microvessels with diameters in the range of about 20-100 μm – the acquisition time needs to be at least 300ms in order to average out noise due to random red blood cell motion and plasma gaps in these microvessels, and their hematocrit is reduced compared to larger vessels. This issue was discussed previously (Sorg et al., 2005). The temporal resolution (dataset acquisition time) can be improved with the use of different filters that have better transmission than liquid crystal tunable filters, and also with more advanced light sources that give control over the distribution of energy in the spectral output, such as the illumination system from OneLight Corporation (MacKinnon et al., 2005).

Combined Multimodal Instrument—We previously reported on a combined wide-field imaging instrument capable of both LSI and multispectral imaging modes (Fig. 10) (Bui et al., 2010). Briefly, the platform utilizes multiple illumination sources, a camera equipped with an electro-optic filter, and a modular design which allows the user to image the dorsal window chamber using broadband transillumination, LSI in epi and transillumination geometries, multispectral imaging in transillumination geometry, and fluorescence imaging in epi-illumination geometry. The multispectral camera utilizes a liquid crystal tunable filter that is removed from the beam path to perform conventional monochrome CCD imaging. The multispectral camera also uses a lens system with interchangeable objectives, allowing imaging at magnifications from 0.5X to 250X. The platform uses two separate helium-neon lasers to perform LSI in epi and transillumination geometries (20 mW and 30 mW, respectively), a 150 W quartz halogen lamp for MSI and broadband transillumination, and a blue LED source centered at 458 nm for fluorescence excitation. Imaging modalities are changed without the need to alter the position of the window chamber preparation or the camera.

REPRESENTATIVE RESULTS

Figure 11 is sample data from a photocoagulation experiment in which selected blood vessels were irradiated and LSI used to determine vascular shutdown and subsequent revascularization. Figure 12 shows both blood flow and hemoglobin saturation in the same dorsal window. This figure demonstrates that LSI and multispectral imaging data are

intrinsically coregistered. Figure 13 shows the effect of using different exposure times in visualizing blood flow in the window chamber. The longer exposure time allows visualization of smaller vessels but is subject to motion artifacts and is less sensitive to faster blood flow.

DISCUSSION

The dorsal window chamber is a very useful and well-established model that enables study of the microvasculature. Here, we present a detailed procedure outlining the surgical installation of the dorsal window chamber, with the goal of enabling researchers to utilize this animal model. Furthermore, we describe the basics of and the procedure to perform wide-field functional imaging of the dorsal window chamber as a complementary technique to intravital microscopy. Specifically, we describe laser speckle imaging and multispectral imaging, wide-field methods which enable interrogation of the hemodynamics and oxygenation of the microvasculature, over larger spatial scales than optical microscopy. We propose that wide-field functional imaging, with its large field of view, can efficiently and effectively guide researchers to select regions of interest in the window chamber preparation to probe subsequently with high-resolution intravital microscopy, as a form of “image-guided microscopy”.

Acknowledgments

This work was supported in part by the Arnold and Mabel Beckman Foundation, a Dean’s Triumvirate Grant from the UC Irvine College of Health Sciences, the National Institutes of Health grant award HD065536, and the National Institutes of Health Laser Microbeam and Medical Program (LAMMP, a P41 Technology Research Resource). Sean White’s effort was supported by a National Science Foundation Graduate Fellowship.

References

- Algire GH. An adaptation of the transparent-chamber technique to the mouse. *J. Natl. Cancer Inst.* 1943; 4:1–11.
- Boas D, Dunn A. Laser speckle contrast imaging in biomedical optics. *J Biomed Opt.* 2010; 15:011109. [PubMed: 20210435]
- Briers J, Fercher A. Retinal blood-flow visualization by means of laser speckle photography. *Invest Ophthalmol Vis Sci.* 1982; 22:255–9. [PubMed: 7056639]
- Briers JD, Webster S. Laser speckle contrast analysis (LASCA): a non-scanning, full-field technique for monitoring capillary blood flow. *J Biomed Opt.* 1996; 1:174–179.
- Bui AK, et al. Longitudinal, multimodal functional imaging of microvascular response to photothermal therapy. *Opt Lett.* 2010; 35:3216–8. [PubMed: 20890338]
- Chao BH, et al. Pre-treatment inflammation induced by TNF-alpha augments cryosurgical injury on human prostate cancer. *Cryobiology.* 2004; 49:10–27. [PubMed: 15265713]
- Cheng H, Duong T. Simplified laser-speckle-imaging analysis method and its application to retinal blood flow imaging. *Opt Lett.* 2007; 32:2188–90. [PubMed: 17671579]
- Cheng H, et al. Modified laser speckle imaging method with improved spatial resolution. *J Biomed Opt.* 2003; 8:559–64. [PubMed: 12880364]
- Cheng H, et al. Temporal statistical analysis of laser speckle images and its application to retinal blood-flow imaging. *Opt Express.* 2008; 16:10214–9. [PubMed: 18607429]
- Chishima T, et al. Cancer invasion and micrometastasis visualized in live tissue by green fluorescent protein expression. *Cancer Res.* 1997; 57:2042–7. [PubMed: 9158003]
- Choi B, et al. The importance of long-term monitoring to evaluate the microvascular response to light-based therapies. *J Invest Dermatol.* 2008; 128:485–8. [PubMed: 17657245]
- Choi B, et al. Laser speckle imaging for monitoring blood flow dynamics in the in vivo rodent dorsal skin fold model. *Microvasc Res.* 2004; 68:143–6. [PubMed: 15313124]

- Choi B, et al. Linear response range characterization and in vivo application of laser speckle imaging of blood flow dynamics. *J Biomed Opt.* 2006; 11:041129. [PubMed: 16965157]
- Dedeugd C, et al. Multimodal optical imaging of microvessel network convective oxygen transport dynamics. *Appl Opt.* 2009; 48:D187–97. [PubMed: 19340108]
- Dellian M, et al. Quantitation and physiological characterization of angiogenic vessels in mice: effect of basic fibroblast growth factor, vascular endothelial growth factor/vascular permeability factor, and host microenvironment. *Am J Pathol.* 1996; 149:59–71. [PubMed: 8686763]
- Dewhirst M, et al. Review of methods used to study oxygen transport at the microcirculatory level. *Int J Cancer.* 2000; 90:237–55. [PubMed: 11091348]
- Dewhirst MW, et al. Quantification of longitudinal tissue pO₂ gradients in window chamber tumours: impact on tumour hypoxia. *Br J Cancer.* 1999; 79:1717–22. [PubMed: 10206282]
- Dreher MR, et al. Tumor vascular permeability, accumulation, and penetration of macromolecular drug carriers. *J Natl Cancer Inst.* 2006; 98:335–44. [PubMed: 16507830]
- Dunn AK, et al. Simultaneous imaging of total cerebral hemoglobin concentration, oxygenation, and blood flow during functional activation. *Opt Lett.* 2003; 28:28–30. [PubMed: 12656525]
- Endrich B, et al. Technical report--a new chamber technique for microvascular studies in unanesthetized hamsters. *Res Exp Med (Berl).* 1980; 177:125–34. [PubMed: 7003665]
- Endrich B, et al. Quantitative studies of microcirculatory function in malignant tissue: influence of temperature on microvascular hemodynamics during the early growth of the BA 1112 rat sarcoma. *Int J Radiat Oncol Biol Phys.* 1979; 5:2021–30. [PubMed: 544581]
- Fercher A, Briers J. Flow Visualization by Means of Single-Exposure Speckle Photography. *Optics Communications.* 1981:326–330.
- Fish, RH. Pharmacology of injectable anesthetics. In: Kohn, DF., et al., editors. *Anesthesia and Analgesia in Laboratory Animals.* Academic Press; New York: 1997. p. 2
- Fukumura D, et al. Tumor induction of VEGF promoter activity in stromal cells. *Cell.* 1998; 94:715–25. [PubMed: 9753319]
- Gaustad JV, et al. Tumor vascularity assessed by magnetic resonance imaging and intravital microscopy imaging. *Neoplasia.* 2008; 10:354–62. [PubMed: 18392132]
- Hardee ME, et al. Novel imaging provides new insights into mechanisms of oxygen transport in tumors. *Curr Mol Med.* 2009; 9:435–41. [PubMed: 19519401]
- Jain R, et al. Dissecting tumour pathophysiology using intravital microscopy. *Nat Rev Cancer.* 2002; 2:266–76. [PubMed: 12001988]
- Jiang J, et al. Tumor necrosis factor-alpha-induced accentuation in cryoinjury: mechanisms in vitro and in vivo. *Mol Cancer Ther.* 2008; 7:2547–55. [PubMed: 18723499]
- Khurana M, et al. Intravital high-resolution optical imaging of individual vessel response to photodynamic treatment. *J Biomed Opt.* 2008; 13:040502. [PubMed: 19021306]
- Kirkpatrick S, et al. Detrimental effects of speckle-pixel size matching in laser speckle contrast imaging. *Opt Lett.* 2008; 33:2886–8. [PubMed: 19079481]
- Laschke MW, Menger MD. In vitro and in vivo approaches to study angiogenesis in the pathophysiology and therapy of endometriosis. *Hum Reprod Update.* 2007; 13:331–42. [PubMed: 17347159]
- Lehr HA, et al. Dorsal skinfold chamber technique for intravital microscopy in nude mice. *Am J Pathol.* 1993; 143:1055–62. [PubMed: 7692730]
- MacKinnon N, et al. Spectrally programmable light engine for in vitro or in vivo molecular imaging and spectroscopy. *Appl Opt.* 2005; 44:2033–40. [PubMed: 15835352]
- Papenfuss HD, et al. A transparent access chamber for the rat dorsal skin fold. *Microvasc Res.* 1979; 18:311–8. [PubMed: 537508]
- Peirce SM, et al. Spatial and temporal control of angiogenesis and arterialization using focal applications of VEGF164 and Ang-1. *Am J Physiol Heart Circ Physiol.* 2004; 286:H918–25. [PubMed: 14604856]
- Pittman R, Duling B. Measurement of percent oxyhemoglobin in the microvasculature. *J Appl Physiol.* 1975; 38:321–7. [PubMed: 1120758]

- Ramirez-San-Juan JC, et al. Impact of velocity distribution assumption on simplified laser speckle imaging equation. *Optics express*. 2008; 16:3197–3203. [PubMed: 18542407]
- Seynhaeve AL, et al. Tumor necrosis factor alpha mediates homogeneous distribution of liposomes in murine melanoma that contributes to a better tumor response. *Cancer Res*. 2007; 67:9455–62. [PubMed: 17909055]
- Shonat R, et al. Near-simultaneous hemoglobin saturation and oxygen tension maps in mouse brain using an AOTF microscope. *Biophys J*. 1997; 73:1223–31. [PubMed: 9284290]
- Sorg B, et al. Spectral imaging facilitates visualization and measurements of unstable and abnormal microvascular oxygen transport in tumors. *J Biomed Opt*. 2008; 13:014026. [PubMed: 18315384]
- Sorg B, et al. Hyperspectral imaging of hemoglobin saturation in tumor microvasculature and tumor hypoxia development. *J Biomed Opt*. 2005; 10:44004. [PubMed: 16178638]
- Vargas G, et al. Use of hyperosmotic chemical agent to improve the laser treatment of cutaneous vascular lesions. *J Biomed Opt*. 2008; 13:021114. [PubMed: 18465963]
- Wu N, et al. Simultaneous measurement of liposome extravasation and content release in tumors. *Microcirculation*. 1997; 4:83–101. [PubMed: 9110286]
- Yuan F, et al. Time-dependent vascular regression and permeability changes in established human tumor xenografts induced by an anti-vascular endothelial growth factor/vascular permeability factor antibody. *Proc Natl Acad Sci U S A*. 1996; 93:14765–70. [PubMed: 8962129]
- Yuan S, et al. Determination of optimal exposure time for imaging of blood flow changes with laser speckle contrast imaging. *Appl Opt*. 2005; 44:1823–30. [PubMed: 15813518]
- Øye KS, et al. A novel method for mapping the heterogeneity in blood supply to normal and malignant tissues in the mouse dorsal window chamber. *Microvasc Res*. 2008; 75:179–87. [PubMed: 17688890]

Research Highlights

- Present detailed protocol to surgically implant dorsal window chamber in mice and hamsters
- Present detailed protocol to perform laser speckle imaging on dorsal window chamber
- Present detailed protocol to perform multispectral oxygenation imaging on dorsal window chamber
- Wide-field optical imaging complements intravital microscopy of dorsal window chamber

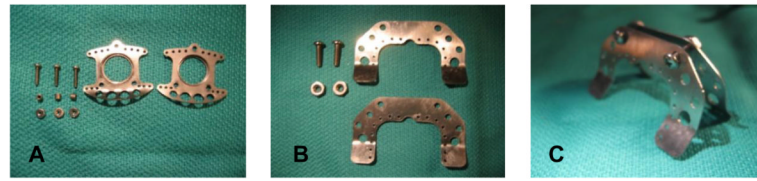


Figure 1.

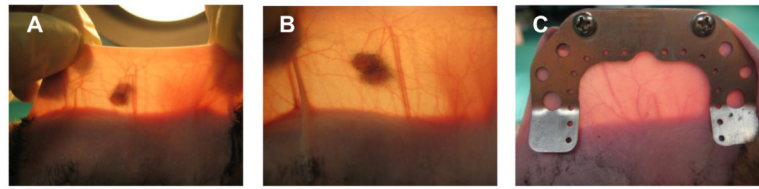


Figure 2.

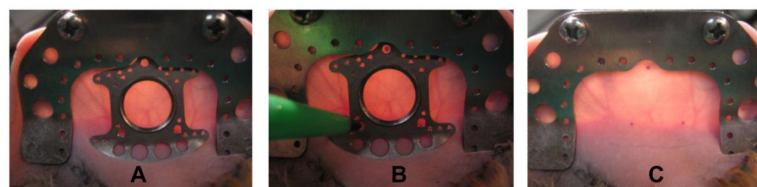


Figure 3.

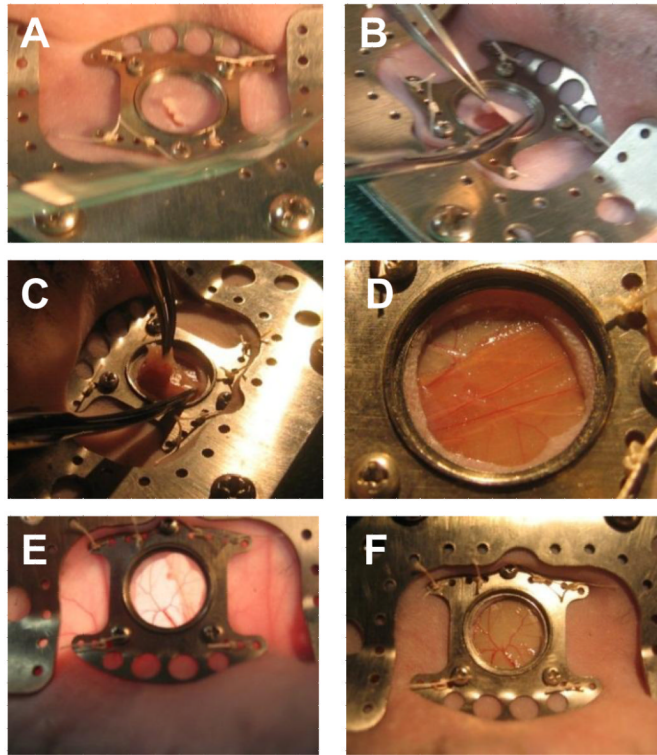


Figure 4.

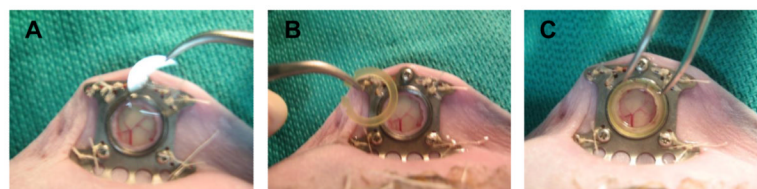


Figure 5.

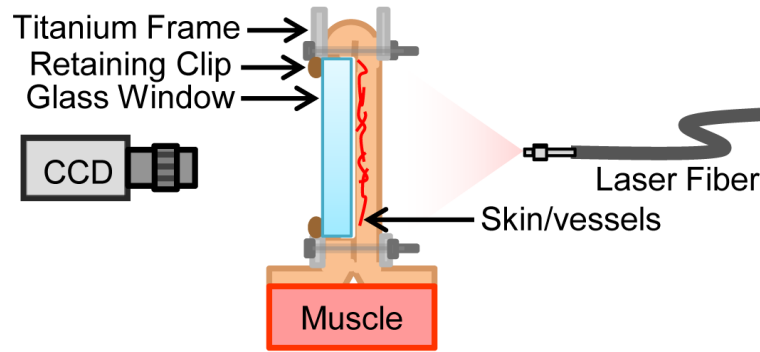


Figure 6.

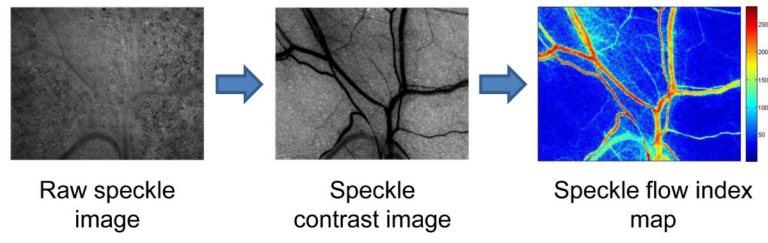


Figure 7.

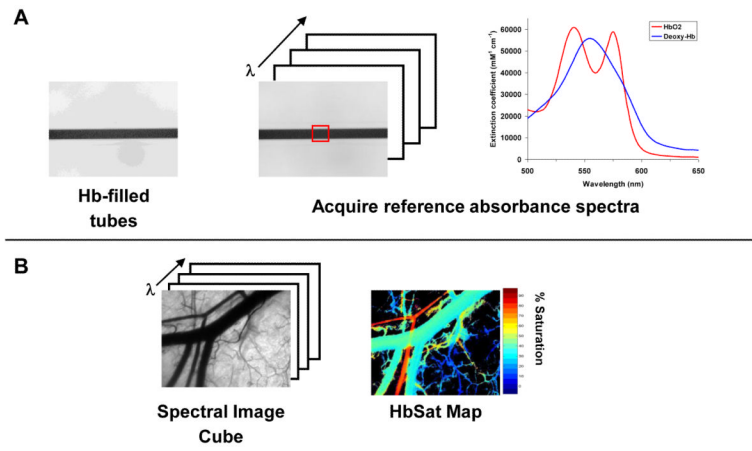


Figure 8.

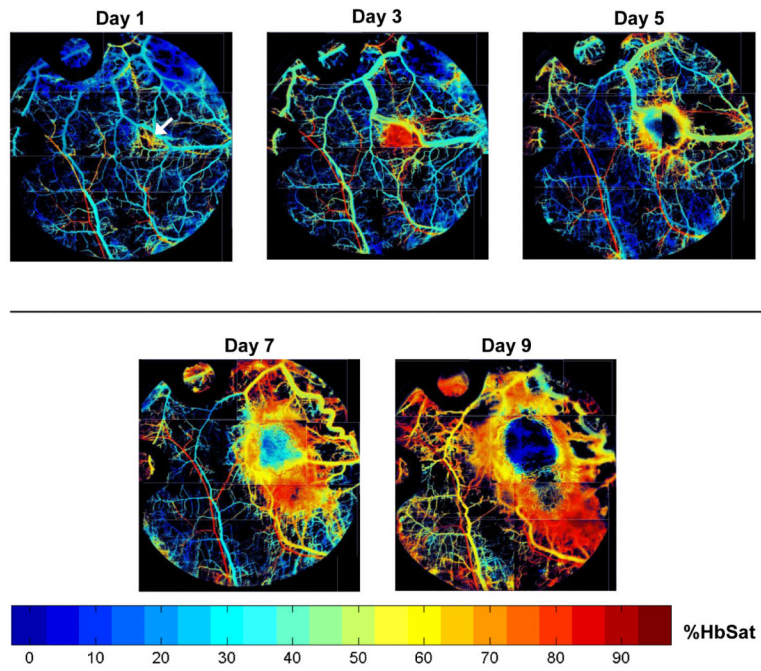


Figure 9.

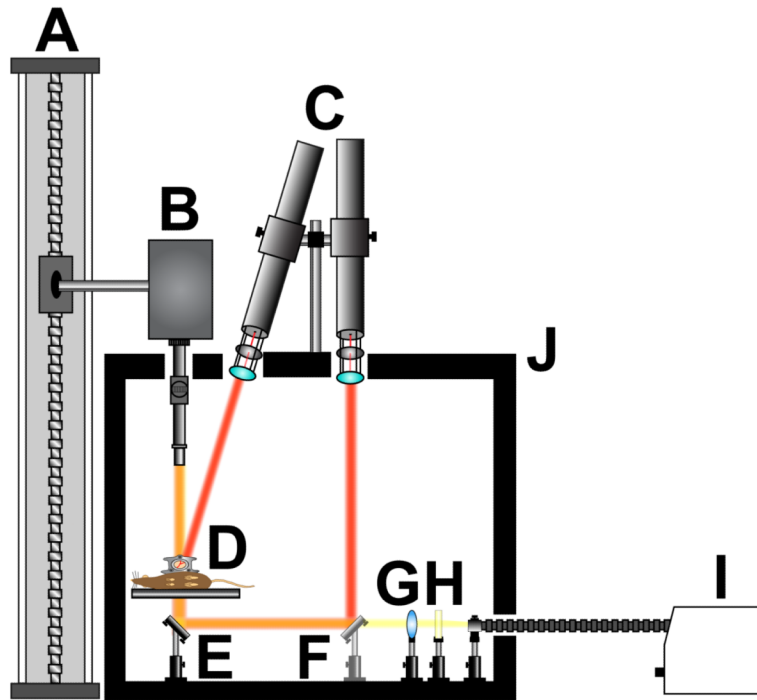


Figure 10.

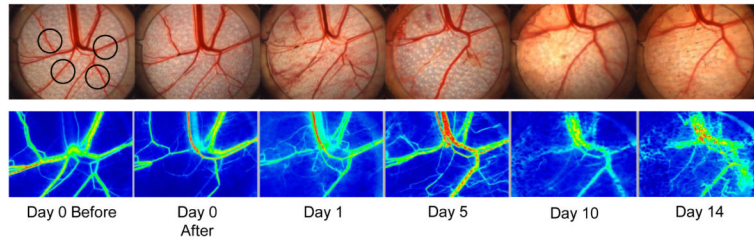


Figure 11.

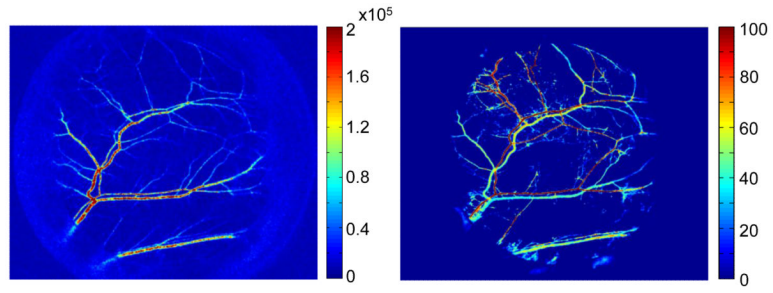


Figure 12.

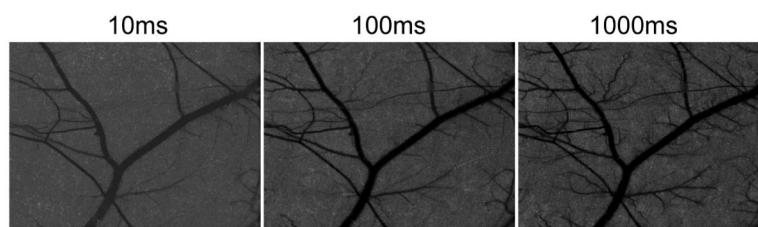


Figure 13.